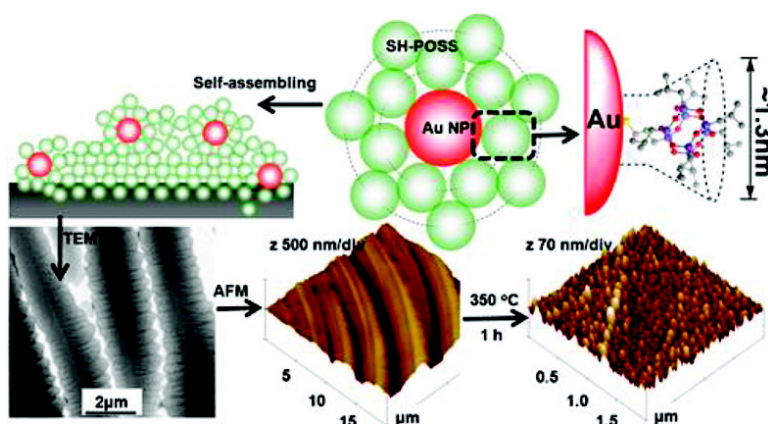Article

Self-Assembled Fernlike Microstructures of Polyhedral Oligomeric Silsesquioxane/Gold Nanoparticle Hybrids

Chu-Hua Lu, Shiao-Wei Kuo, Chih-Feng Huang, and Feng-Chih Chang

More About This Article

Additional resources and features associated with this article are available within the HTML version:

- Supporting Information
- Access to high resolution figures
- Links to articles and content related to this article
- Copyright permission to reproduce figures and/or text from this article

View the Full Text HTML

Self-Assembled Fernlike Microstructures of Polyhedral Oligomeric Silsesquioxane/Gold Nanoparticle Hybrids

Chu-Hua Lu,[†] Shiao-Wei Kuo,[‡] Chih-Feng Huang,[†] and Feng-Chih Chang*,[†]

Institute of Applied Chemistry, National Chiao Tung University, 30010 Hsinchu, Taiwan, and Department of Materials and Optoelectronic Science, Center for Nanoscience and Nanotechnology, National Sun Yat-Sen University, 804 Kaohsiung, Taiwan

Received: September 29, 2008; Revised Manuscript Received: December 15, 2008

We have used a thiol-functionalized polyhedral oligomeric silsesquioxane (SH-POSS) as a protective group for the preparation of POSS-protected gold nanoparticles (POSS–Au NPs). The organic/inorganic hybrid SH-POSS NPs exhibited an interesting platelike morphology arising from steric hindrance between the isobutyl groups of SH-POSS. An XRD study of the SH-POSS crystal revealed the relatively large interstice (1.64 nm lattice constant *a* > 1.3 nm diameter SH-POSS) on the basal plane of the unit cell, which resulted in a platelike morphology having lateral dimensions on the order of a few micrometers and thicknesses of a few hundred nanometers. In addition to behaving as a stabilizer for the preparation of Au NPs, an excess of SH-POSS colloids led to the formation of a crystalline template that incorporated the POSS–Au hybrid NPs on its surface, providing a unique fernlike microstructure. After removal of the POSS template (through sublimation and decomposition to a silica char) at 350 °C in air for 1 h, nanosized Au islands having diameters of 50–100 nm and thicknesses of 2–20 nm were sintered onto the substrate. As a result, SH-POSS is an excellent protective group for the preparation of Au NPs of high stability in the powder state. In addition, we suspect that SH-POSS crystals could be used to disperse Au NPs onto substrates for a wide range of applications (e.g., Au catalysts).

1. Introduction

Self-assembly of nanoparticles (NPs)—i.e., the controlled organization of NPs into ordered or hierarchical structures—allows coupling of their size- and shape-dependent properties to obtain potentially useful materials for optoelectronics, sensing and imaging, and biomedical applications.[1-4] A broad range of targeted self-assembled structures can be produced by organizing NPs exhibiting compositional heterogeneity.[5-8] They can be realized either by synthesizing NPs from several different materials or by selectively attaching organic molecules to different sites of the NPs.[9-11] Compositional heterogeneity makes NPs conceptually similar to amphiphilic molecules (e.g., surfactants or block copolymers) and allows the thermodynamic approach of self-assembly to be used to form "colloidal molecules" in energetically favorable structures possessing unique properties.[12-22] Ordered monolayers of NPs over large surface areas are sensitive to the presence of defects on the substrate's surface, which can destroy the assembly. In contrast, large ordered arrays of NPs can be obtained through judicious choice of the types of chemical interactions between the particles and the substrate.[23,24] In this paper, we report the preparation of ordered fernlike 3D microstructures of assembled POSS–Au hybrid NPs onto a large-scale crystalline POSS template. Alkyl-functionalized polyhedral oligomeric silsesquioxane (alkyl POSS) derivatives are well-known organic/inorganic hybrid NPs comprising 0.5 nm diameter siloxane cages and eight alkyl chains.[25] Thus, alkyl POSS molecules can be regarded as colloids (a dispersed phase and a dispersion medium) in solution. Interestingly, platelike morphologies of POSS crystals, with

lateral dimensions on the order of a few micrometers and thicknesses of a few hundred nanometers, have been described several times previously.[26-29] Therefore, in this study, we employed a thiol-functionalized POSS as (i) a protective group to stabilize Au NPs in solution and (ii) a novel template for the incorporation of Au NPs into thin films.

Thiol compounds are often used to form monolayers on the surfaces of Au NPs via the formation of dynamic S–Au covalent bonds.[30] The concentration of the Au NPs is usually maintained at less than 5 wt % to prevent irreversible aggregation. Thus, the self-assembly of Au NPs in condensed phases is difficult because of the strong tendency to form a concentrated droplet, rather than a large-scale thin film, during evaporation of the solvent. Schmid et al. used 3-mercaptopropylcyclopentyl–POSS to quantitatively exchange the PPh₃ ligands in $(PPh_3)_{12}Au_{55}Cl_6$ in an attempt to obtain POSS–Au NPs stabilized through Au–S bonds; instead, they obtained amorphous structures.[31] Naka et al.[32,33] and Rotello et al.[34,35] have prepared POSS–Au hybrid NPs that were stabilized through electrostatic interactions with the HCl salts of octa(3-aminopropyl)octasilsesquioxane or through hydrogen bonding recognition processes with diaminopyridine-monofunctionalized octasilsesquioxane. Such strong intermolecular interactions (i.e., electrostatic and hydrogen bonding interactions) would suppress the thin-film character of POSS during crystallization. In an attempt to exploit the "crystalline template" of alkyl POSS colloids to self-assemble Au NPs, we turned our attention toward the use of a thiol-monofunctionalized 3-mercaptopropylisobutyl–POSS (herein denoted "SH-POSS"; Figure 1a). We synthesized SH-POSS-protected Au NPs (POSS–Au) using the method developed by Brust et al., in which HAuCl₄ was transferred into the toluene phase with tetraoctylammonium bromide (TOAB) and then reduced with sodium borohydride (NaBH₄) in the presence of

---
* Corresponding author. E-mail: changfc@mail.nctu.edu.tw.
† National Chiao Tung University.
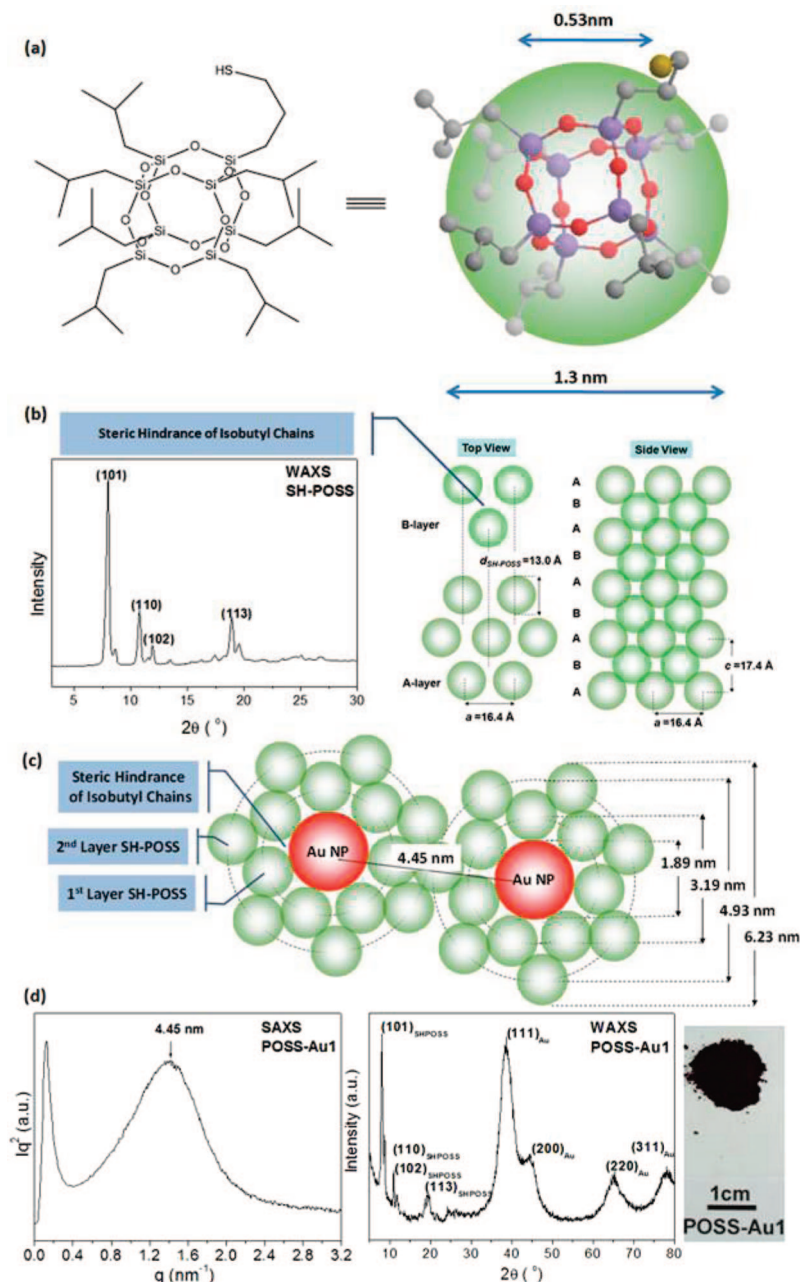‡ National Sun Yat-Sen University.

Figure 1. (a) Chemical structure and 3D model of SH-POSS. (b) WAXS spectrum and cartoon representation of the molecular packing in a SH-POSS crystal. (c) Cartoon representation of the molecular packing in the SH-POSS bilayer-protected POSS−Au1, with the center-to-center distance between two Au cores highlighted. (d) SAXS and WAXS spectra of POSS−Au1 powders. The insert photograph is crystal powder of POSS−Au1.

SH-POSS.[36,37] Thus, interesting large-scale POSS−Au hybrid microstructures[36,38]—featuring 2∼4 nm diameter Au NPs surrounded by 1.3 nm diameter POSS colloids—could be constructed from a crystalline POSS template (an excess of SH-POSS).[33−35] In addition, at temperatures above 250 °C, most alkyl POSS derivatives can be sublimed, with the residual alkyl POSS (ca. 7.5 wt %) decomposing and oxidizing into a silica char (a network of POSS cages).[39,40] Therefore, we obtained Au-island films through subsequent sintering of well-dispersed Au NPs on the large fernlike microstructures in air at 350 °C.

In this study, we first investigated the characteristic of SH-POSS crystals using power X-ray diffraction analysis. We found that steric hindrance of the alkyl groups on the POSS cages dominated the formation of fernlike or dendritic crystals and provided relatively large interstices on the crystal surface, similar to those observed for NH_4Cl, NH_4Br, and CsCl crystals because

of large interstices resulting from ionic repulsion between halide anions.[41] We suspected that it would be reasonable to self-assemble POSS-surrounded Au NPs onto the relatively large interstices on the surface of excess SH-POSS crystals because of the strong tendency for POSS units to aggregate. This novel template—the SH-POSS crystal—can form on several substrates, including water, silicon wafers, and glass slides. Because of its easy and reproducible sample preparation process, the fernlike microstructures of the POSS−Au hybrids can be analyzed using many microscopic techniques, including transmission electron microscopy (TEM), scanning electron microscopy (SEM), atomic force microscopy (AFM), and optical microscopy (OM).

2. Results and Discussion

2.1. POSS Crystals on Au NPs. Although it is difficult to evaluate the exact size of an alkyl POSS derivative because of

POSS−Au Fernlike Hybrids

J. Phys. Chem. C, Vol. 113, No. 9, 2009 **3519**

the flexibility of the alkyl chain, the total diagonal length of alkyl POSS can be considered as a measure of its size. SH-POSS can be regarded as a 1.3 nm diameter organic/inorganic hybrid colloid ($d_{SH-POSS}$) because it possesses 0.4 nm long isobutyl chains on its 0.53 nm diameter inorganic siloxane cage.[21,32,42] Once the critical particle concentration is reached, a sharp transition from dispersed colloids to a condensed crystalline-like behavior is observed. The transition from the colloid liquid (dispersed state) to the colloidal crystalline phase (condensed state) is first order in nature, similar to the phase transitions from liquid to solid observed in molecular systems.[43] Thus, the crystallography of the condensed POSS state can also be studied through X-ray diffraction analyses (XRD). Figure 1b reveals that the powder XRD (wavelength: 1.5418 Å) patterns of the SH-POSS crystals displayed four major diffraction angles (2θ) and *d*-spacing distances (d_{hkl})—8.03° (11.00 Å), 10.78° (8.20 Å), 11.92° (7.42 Å), and 18.73° (4.69 Å)—that corresponded to the (*hkl*) diffraction planes (101), (110), (102), and (113) for a hexagonal POSS crystal with the following lattice parameters: $\gamma = 120°$; $\alpha = \beta = 90°$. According to the hexagonal unit cell, the lattice parameters ($a = b = 16.4$ Å; $c = 17.4$ Å) were calculated using eq 1. When the crystalline model of the 1.3 nm diameter SH-POSS spheres was made (Figure 1b), we observed relatively large interstices (lattice parameter *a* of 16.4 Å > SH-POSS diameter of 1.3 nm) on the basal plane of a SH-POSS unit cell. For hexagonal close packing (HCP) of hard spheres having a diameter d_s, eq 2 suggests that the *z*-pitch distance (d_z) of the ABA repeating layers in the axial direction is $0.816 \times d_s$. Herein, the lattice parameters *a* and *c* for HCP are equal to the diameter of the hard spheres (d_s) and twice the *z*-pitch distance ($2d_z$) for the two repeating layers, respectively. Thus, the dimensional ratio *c/a* for HCP is calculated to be 1.63.

Assuming nonoverlapping packing in the axial direction (*z* direction), eq 3 suggests that the theoretical *z*-pitch distance (d_z^*) of an SH-POSS crystal is 8.91 Å, a value larger than the experimental (Figure 1b) *z*-pitch distance ($d_{z,SH-POSS}$) of 8.7 Å (i.e., lattice parameter *c*/2). Unlike the HCP of hard spheres, we speculate that the substrate-supported SH-POSS colloids can approach one another to pack into the basal plane with a relatively large interstice of a crystal. Because of repulsion between the sterically demanding isobutyl groups on the POSS cages, the intermolecular distance is slightly larger than the diameter of the SH-POSS colloid. The free SH-POSS colloid in solution can then pack onto the surface interstices of the first layer. For nonsupported free SH-POSS colloids, the soft organic shell of SH-POSS colloids can overlap slightly with the low-level SH-POSS colloids, forming a three-dimensional crystal. Thus, the dimension *c/a* of SH-POSS crystal is calculated to be 1.06 for platelike unit cells (i.e., less than the value of 1.63 for the HCP of hard spheres). In addition, the difference in the intermolecular distances between the basal plane and the axial direction results in major crystal growth in two approximately orthogonal directions parallel to the substrate, leading to the ordered aggregation of platelike unit cells into fernlike or dendritic crystals having lateral dimensions on the order of a few micrometers and thicknesses of a few hundred nanometers.[26−29]

Steric interactions of the alkyl chains on the POSS cages appear to dominate the low dimensional ratio *c/a* (1.06 < 1.63) of the unit cell of a SH-POSS crystal. For bulky molecules without alkyl chains, C_{60}[44,45] molecules and octahydro-POSS [$(HSiO_{1.5})_8$, 424.74 g/mol][46] possess lattice dimensional ratios (*c/a*) of 1.62 and 1.68, respectively, in their hexagonal unit cells—values quite close to the idea dimensional ratio (1.63)

expected for the HCP of hard spheres. Fernlike and dendritic crystals of inorganic salts, such as NH_4Cl, NH_4Br, and $CsCl$, are commonly observed.[41] In these cases, repulsion of hydrated halide anions induces loose packing on the basal plane of a unit cell, allowing cations to insert into the kink sites (interstices) after dehydration. Thus, we infer that the formation of fernlike or dendritic SH-POSS crystals was dominated by steric hindrance between the solvated isobutyl chains on the POSS cages.

$$\frac{1}{d_{hkl}^2} = \frac{4}{3}\left(\frac{h^2 + hk + k^2}{a^2}\right) + \frac{l^2}{c^2} \quad (1)$$

$$d_z = \sqrt{d_s^2 - d_s^2/3} \quad (2)$$

$$d_z^* = \sqrt{d_s^2 - a^2/3} \quad (3)$$

2.2. Character of POSS−Au Hybrids. Because bulky SH-POSS colloids can pack loosely into crystals on various substrates, we expected them to be excellent protective agents for the dispersion of Au NPs after becoming anchored onto their surfaces through Au−S bonds. We synthesized the SH-POSS-protected Au NPs (POSS−Au) through the reduction of $HAuCl_4$ in the presence of SH-POSS. Because $HAuCl_4$ is water soluble, a phase-transfer agent (TOAB) was required to transfer it into the toluene phase. TOAB also transfers the reducing agent ($NaBH_4$) into toluene. Using this approach, we obtained POSS−Au1 and POSS−Au2 at $HAuCl_4$-to-SH-POSS feeding molar ratios (*n:m*) of 1:1 and 1:0.5, respectively. 1-Dodecanethiol (C12-SH)-protected Au NPs (C12−Au; *n:m* = 1:1) were also prepared as a control. We used many techniques to analyze our POSS−Au and C12−Au hybrid NPs—OM, SEM, TEM, AFM, Fourier transform infrared (FTIR) spectroscopy, ESCA, small-angle X-ray scattering (SAXS), wide-angle X-ray scattering (WAXS), dynamic light scattering (DLS), and thermogravimetric analysis (TGA) (see the Supporting Information for additional details). Because Au atoms scatter electrons efficiently as a result of their high mass number, the sizes of the Au cores are easily measured using TEM (i.e., high contrast between the Au NPs and thiol compounds). To disperse the POSS−Au or C12−Au NPs, we prepared dilute samples for TEM imaging by (i) placing a drop of dilute solution (1 mg/mL) onto a carbon-coated copper grid, (ii) blotting away the excess solution using a strip of filter paper, and (iii) air-drying at 25 °C for 3 min. Thus, through statistical analysis using the Gatan image process, we obtained Au core sizes for C12−Au, POSS−Au1, and POSS−Au2 of 2.0 ± 0.7, 1.8 ± 0.9, and 2.8 ± 0.9 nm, respectively. These values suggest that SH-POSS plays the same role as that of the well-known C12-SH for the dispersion of Au NPs in toluene.[31]

In addition to the dispersed state, we also studied the condensed states of POSS−Au and C12−Au.[43] After evaporation of the toluene, we extracted TOAB and excess $NaBH_4$ into methanol to obtain a pure powder for POSS−Au1 and a sticky material for C12−Au. On the basis of their char yields at 700 °C, TGA revealed *n/m* ratios for POSS−Au1 and C12−Au of 2.76 and 2.61, respectively. Thus, in the preparation of Au NPs using the water/toluene two-phase method,[36,37] the loss of SH-POSS and C12-SH resulted in higher experimental *n/m* ratios for both POSS−Au1 and C12−Au. With its low content of SH-POSS, we could not purify POSS−Au2 because the amorphous SH-POSS units became redispersed in methanol. Theoretically, if most SH-POSS colloids are bound onto the spherical surfaces of Au NPs, crystallization of SH-POSS colloids would be suppressed, as was the case for POSS−Au2. In contrast, POSS−Au1 was a powder-like crystal (see the inserted graphs
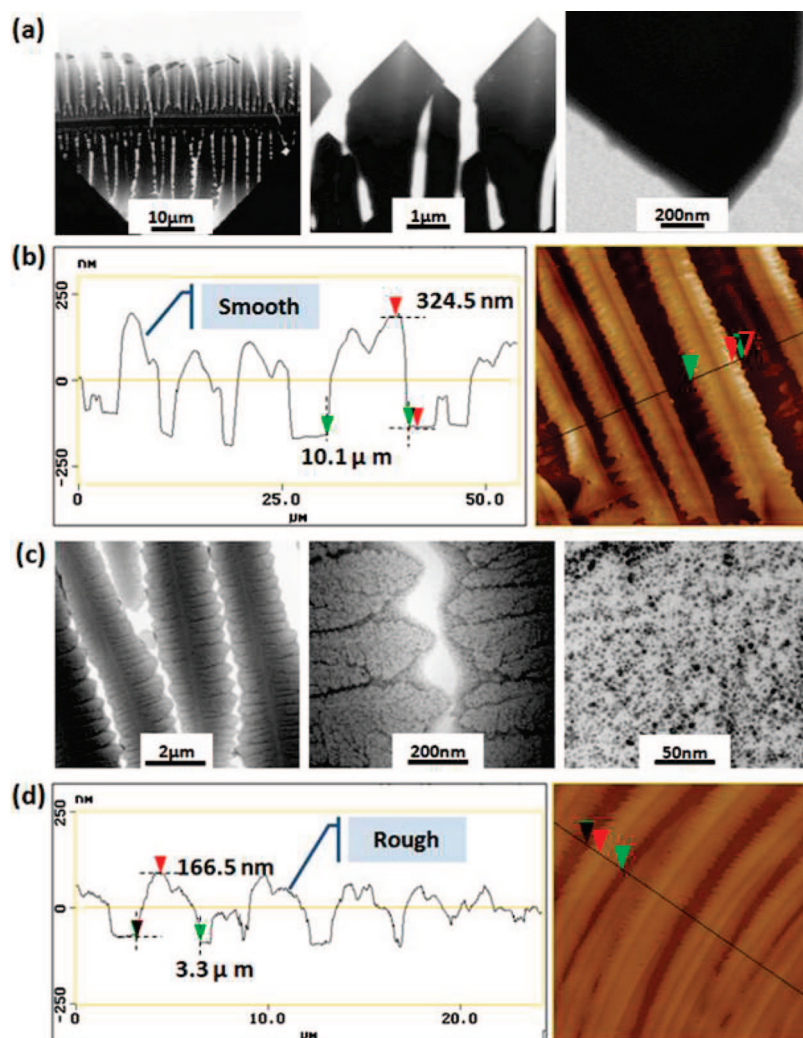
Figure 2. TEM images, (various) magnifications, and AFM sectional analyses of the (a, b) SH-POSS and (c, d) POSS−Au1 fernlike microstructures.

in Figure 1d). Thus, we needed to determine the packing mode of the SH-POSS colloids on the spherical surface of Au NPs (Figure 1c). The number of SH-POSS colloids absorbed on the surface of each Au NP can be calculated in terms of the n/m ratio, based on the bulk Au density of 19.3 g/cm^3 and the packing mode of a SH-POSS crystal. Because of the large interstices on the basal plane of a SH-POSS unit cell, we supposed that the SH-POSS colloids would pack into a bilayer shell on the surfaces of the Au cores, thereby reducing thermodynamically disfavored contact between the Au cores and toluene (Figure 1c). The SH-POSS colloids in the first layer are chemically absorbed onto the Au cores through Au−S bonds; in contrast, those in the second layer can be classified as physically absorbed through POSS−POSS recognition.[35] As a result, the theoretical n/m ratios of POSS−Au1 were 14.48 and 4.24 for the monolayer and bilayer, respectively, of 1.3 nm diameter SH-POSS spheres surrounding 1.84 nm diameter Au cores. To determine the mode of assembly of the SH-POSS bilayer on the Au core, we performed a SAXS study on the POSS−Au1 powder (Figure 1d). The broadband at a scattering vector (q) of 1.41 nm^{-1} corresponds to a spacing distance of 4.45 nm, indicating the center-to-center distance between two Au cores. Thus, the surface-to-surface distance of 2.60 nm can be assigned to the aggregation of the protective POSS bilayer encapsulating 1.84 nm diameter Au NPs.[19] In addition, DLS analysis of POSS−Au1 revealed an average size (D_h) of 7.9

nm, slightly larger than the predicted size (6.23 nm) because of reversible absorption of toluene-solvated SH-POSS colloids onto the surfaces of the Au NPs (see Figure S12 in the Supporting Information). We also performed WAXS (Figure 1d) analyses to ensure that the feeding of SH-POSS was more than that required for the POSS-bilayer-protected Au NPs to form a "pure" SH-POSS crystal. In addition to the four sharp diffraction bands for the hexagonal POSS crystal, the WAXS spectrum of POSS−Au1 displayed another four broad diffraction angles (2θ) and d-spacing distances (d_{hkl})—38.60° (2.33 Å), 44.43° (2.04 Å), 65.10° (1.43 Å), and 78.01° (1.22 Å)—corresponding to the (hkl) diffraction planes (111), (200), (220), and (311) for a face-centered cubic (FCC) lattice Au phase.[47] Thus, the excess SH-POSS colloids play an important role in the aggregation of the POSS−Au hybrid NPs. Moreover, the powder POSS−Au1 containing bulky POSS exhibited higher stability for long-term storage than did C12−Au because the dynamic nature of the Au−S bonds led to local aggregation through exchange of thiol-functional ligands (see Figures S9 and S15, Supporting Information). The repulsion interaction between POSS colloids can prevent the exchange of Au−S bonds to stabilize Au NPs.

2.3. TEM and AFM Analyses of POSS−Au Micro- and Nanostructures. Because the theoretical n/m ratio was 4.24, the low experimental (TGA) ratio of 2.76 for POSS−Au1 indicates the presence of an excess of SH-POSS colloids. During solvent evaporation, excess SH-POSS colloids have a strong
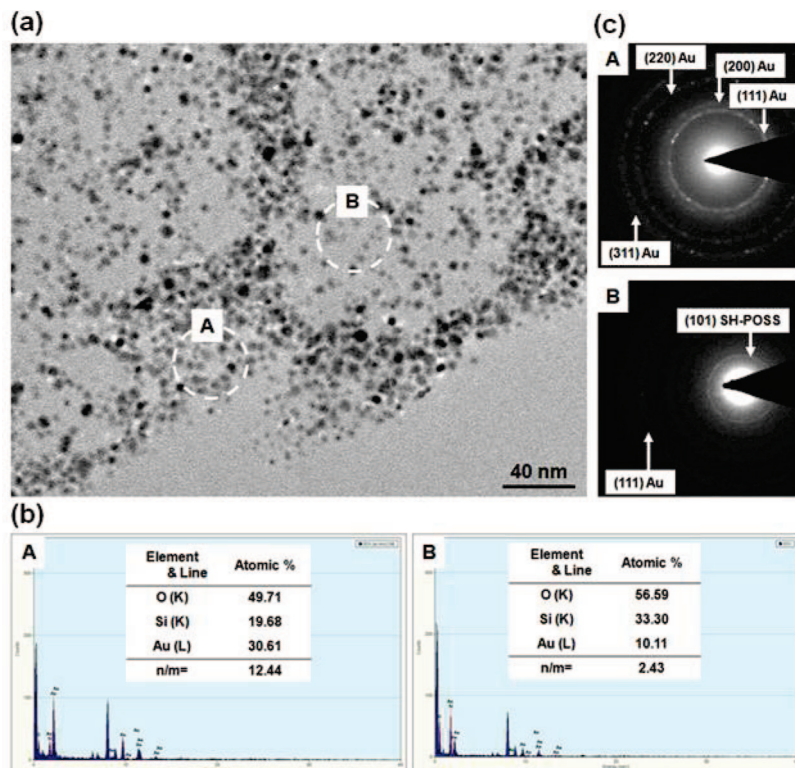
POSS−Au Fernlike Hybrids

J. Phys. Chem. C, Vol. 113, No. 9, 2009 **3521**

Figure 3. (a) HRTEM image, (b) energy dispersive X-ray spectra, and (c) electron diffraction patterns of the POSS−Au1 aggregate. Regions A and B are rich and poor in the Au component, respectively.

tendency to crystallize (thermodynamic first-order phase transition) prior to aggregation of the POSS−Au hybrid NPs. As mentioned above, the crystallization of SH-POSS colloids leads to fernlike or dendritic crystalline morphologies having lateral dimensions on the order of a few micrometers and thickness of a few hundred nanometers. Theoretically, the crystallization of excess SH-POSS colloids should lead toward macrophase separation from the POSS−Au hybrid NPs. We observe, however, fernlike microstructures for both SH-POSS and POSS−Au1 (feeding ratio, $n:m$ = 1:1). Thus, we used TEM to investigate the condensed morphologies of SH-POSS and POSS−Au1 (because of the high contrast between Au and SH-POSS) and AFM to observe the 3D topologies of the crystalline microstructures (Figure 2). Samples were prepared by evaporating one drop of a dilute toluene solution (10 mg/mL for POSS−Au1; 50 mg/mL for SH-POSS) on a water surface (for TEM) and on a wafer (for AFM). After evaporating the toluene at 25 °C for 30 min, we transferred the samples to a carbon-coated Cu TEM grid for TEM analyses. At low magnification, individual micrometer-long and -wide ferns were visible for both SH-POSS and POSS−Au1 (Figures 2a and 2c). At higher magnification of POSS−Au1, we could distinguish dark spots (Au cores), some of which were aggregated along the boundary of the fernlike microstructure, resulting in the dark boundary observed at low magnification. AFM analyses (sectional analyses and 2D images) revealed fernlike microstructures for SH-POSS and POSS−Au1 (Figures 2b and 2d), similar to those observed by TEM (Figures 2a and 2c). The fernlike microstructures of SH-POSS and POSS−Au1 were ca. 10.1 and 3.3 μm wide; the detected tapes heights were 324.5 and 166.5 nm, respectively. We attribute the smaller sizes of the fernlike microstructures for POSS−Au1 to suppressed SH-POSS crystallization with POSS−Au hybrid NPs. In addition, the rough surface of POSS−Au1 (Figure 2d) indicates the incorporation of 6.23 nm diameter Au NPs onto the surface of the crystalline POSS

template. We suspect that the relatively large interstices on the surface of the SH-POSS fernlike template allow the incorporation of SH-POSS on the surface of the Au cores through POSS−POSS recognition processes.[35]

We used multifunctional high-resolution TEM (HRTEM) to investigate the elemental composition between the boundary and internal regions. The TEM image clearly displays a different distribution of Au cores in these two regions (Figure 3a). Analysis of TEM-assisted energy dispersive X-ray spectra (TEM-EDX) provided the resulting n/m ratios of Au atoms to SH-POSS molecules of 12.44 and 2.43 for the Au-rich boundary (region A) and Au-poor internal (region B) zones (Figure 3b). In comparison with the expected n/m ratios of 14.48 and 4.24 for monolayer and bilayer packing of SH-POSS spheres, we suspect that the packing of SH-POSS for the POSS−Au hybrid NPs should occur in the form of a monolayer in region A and a bilayer in region B. In addition, the relatively low n/m ratios in both regions A and B indicate that the interparticle region is filled with excess SH-POSS colloids. We recorded electron diffraction patterns at regions A and B to investigate the crystallization behavior of the Au atoms and SH-POSS colloids. In region A, four electron diffraction bands of Au NPs are visible (Figure 3c); they agree with our results from the powder WAXS analysis (Figure 1d). In region B, the relatively intense band at low diffraction angle corresponds to the (101) diffraction plane of the SH-POSS crystals and the (111) plane of the Au NPs. As a result, excess SH-POSS colloids in internal region B should form a crystal template for inserting POSS−Au hybrid NPs with bilayer POSS. Upon reducing the concentration of SH-POSS colloids to form the template of a SH-POSS crystal, physically absorbed SH-POSS on the second layer of the POSS−Au hybrid NPs would be released to form a POSS-protective monolayer encapsulating 1.84 nm diameter Au NPs, followed by aggregation in region A.
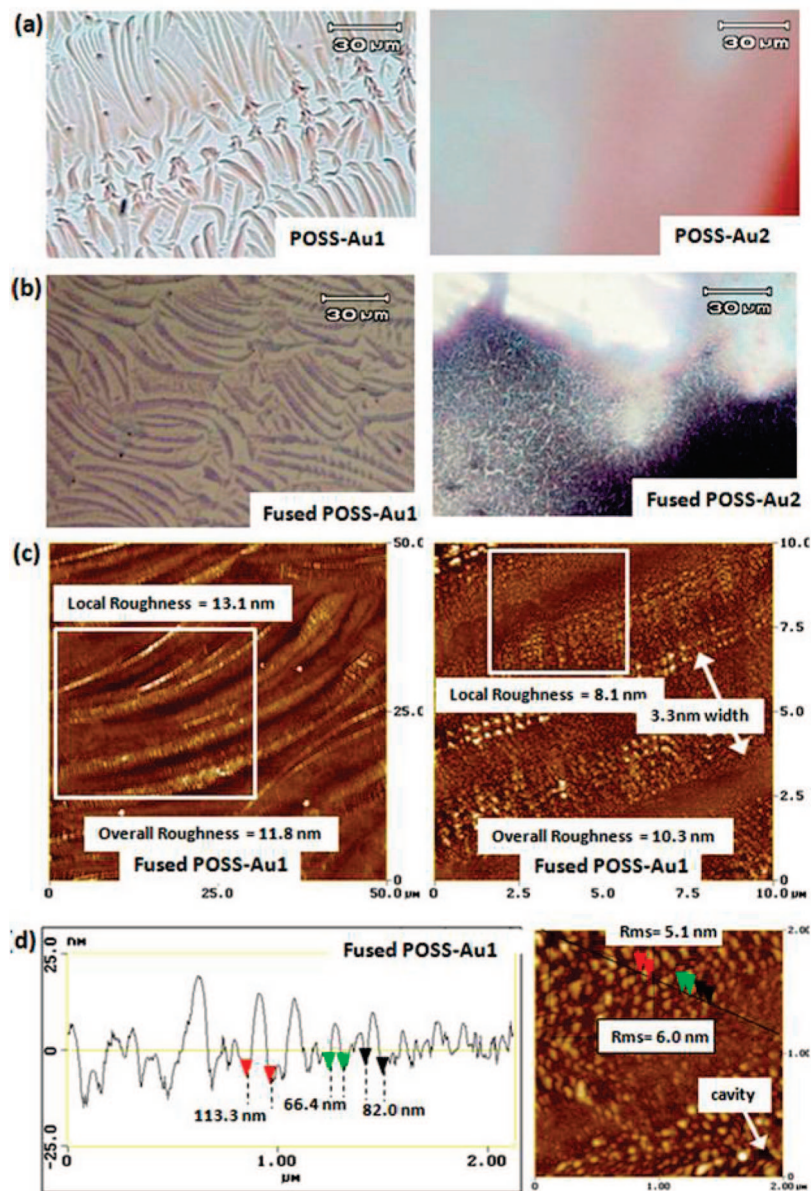
Figure 4. (a, b) OM images (× 500) of POSS−Au1 and POSS−Au2 (a) before and (b) after thermal fusion at 350 °C for 1 h. (c) AFM 2D images of heat-fused POSS−Au1 viewed at scales of 50 × 50 μm^2 and 10 × 10 μm^2. (d) AFM sectional analysis of heat-fused POSS−Au1 viewed at a scale of 2 × 2 μm^2.

2.4. Thermal Sintering of POSS−Au Micro- and Nanostructures. This method using a POSS crystalline template is easy to scale up for bulk-quantity synthesis of POSS−Au microwires; these aggregated NPs can be fused together through thermal treatment. At temperatures above 250 °C, 92.5 wt % of the SH-POSS molecules undergo sublimation, and the remaining molecules decompose and oxidize into a silica char with a network of POSS cages.[39,40] Figure 4a displays an OM image of the reddish fernlike microwires obtained after drying one drop of a dilute (10 mg/mL) POSS−Au1 (feeding ratio *n:m* = 1:1, with excess SH-POSS) solution on a glass slide. In contrast, POSS−Au2 (feeding ratio *n:m* = 1:0.5) was a droplike liquid because the number of SH-POSS colloids was insufficient to form the POSS crystal template. This observation also indicates that excess SH-POSS can disperse Au NPs onto the substrate. In contrast to the slight shrinkage that occurred when the Au film for POSS−Au2 was placed in an oven at 350 °C in air for 1 h, the resulting calcined POSS−Au1 turned purple and resembled metallic Au NPs (Figure 4b). In addition, the

char yields of SH-POSS are 3.1 and 7.5 wt % in nitrogen and air, respectively (see Figure S6, Supporting Information); in contrast, the char yields of POSS−Au1 were 39.7 and 54.5 wt %, respectively, suggesting that the greater silica char in air (oxidation by oxygen) constitutes larger interparticle grain boundaries between fused Au NPs (Figure 4c).[48,49] 2D AFM images of the large-scale aggregation (50 × 50 μm^2) of heat-fused POSS−Au1 revealed significant 11.8 nm overall and 13.1 nm local surface roughnesses. On the scale of 10 × 10 μm^2, individual fernlike microwires (ca. 3.3 μm wide) were also visible, corresponding to the POSS−Au1 fernlike microstructures in Figure 2d. The particle sizes of the fused Au NPs could also be calculated through sectional analyses on the scale of 2 × 2 μm^2. The films possessed nanoscale Au islands having thicknesses of 2−20 nm and diameters of 50−100 nm on the substrate resulting from fusion of dispersed Au NPs (Figure 4d). Moreover, the many cavities present in the Au-rich regions indicate that fusion of the Au NPs occurred to form a porous bulk Au network upon the sublimation of SH-POSS. Although
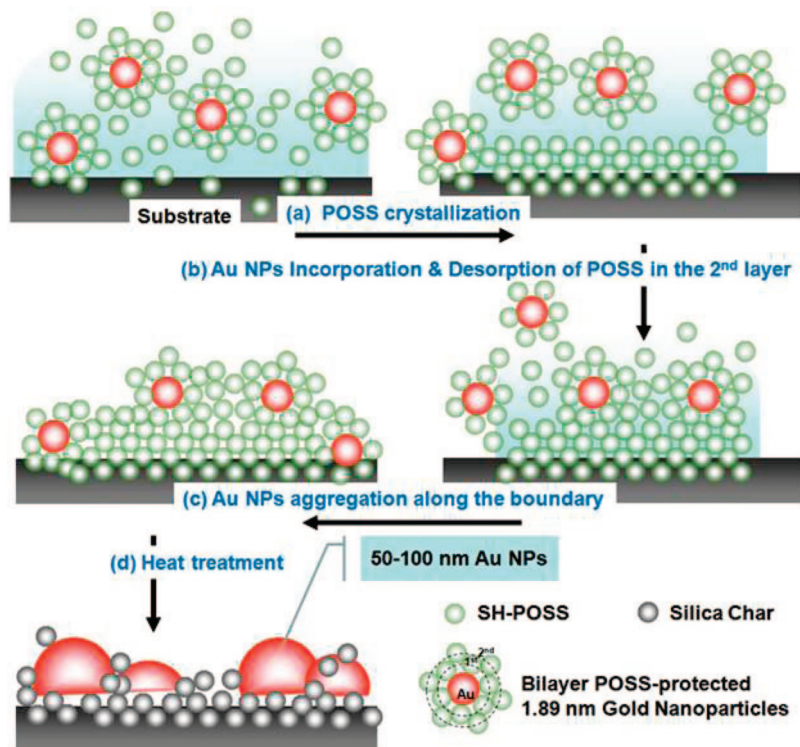
POSS−Au Fernlike Hybrids

J. Phys. Chem. C, Vol. 113, No. 9, 2009 **3523**

Figure 5. Schematic representation of the formation of fernlike POSS−Au1 microstructures.

similar Au-island films can be obtained through resistive thermal evaporation (physical vapor deposition) onto glass substrate,[50] our present technique (using a novel SH-POSS crystalline template) is a simpler and more effective method for preparing Au-island films.

2.5. Mechanism of Formation of POSS−Au Hybrids. On the basis of the microscopic data and existing understanding of alkyl−POSS crystals, we propose the following structural model for the formation of the fernlike hybrid microstructures (Figure 5). As a result of steric interactions between its isobutyl side groups, SH-POSS packs into a bilayer shell on the surface of the Au cores, resulting in the high dispersion of the POSS−Au NPs in toluene. During the process of solvent evaporation, excess SH-POSS colloids (i.e., those not bound onto Au cores) tend to pack in the form of fern- and platelike crystals that function as templates for the self-assembly of POSS−Au NPs onto the surface interstices of the SH-POSS crystals. Upon reducing the SH-POSS concentration in toluene, the SH-POSS colloids on the second layer of the bilayer of the POSS−Au NPs are released to fill the gaps between the incorporated Au NPs. Finally, the monolayer-protected POSS−Au NPs aggregated at the boundaries of the fern micropatterns, resulting in the POSS−Au NP hybrid fernlike micropatterns. When the samples were placed in an oven at 350 °C in air, the SH-POSS molecules either underwent sublimation or their organic alkyl chains decomposed, followed by oxidation and gelation into a silica char. As a result, a porous metallic network was obtained through the sintering of the Au NPs on the substrate.

3. Conclusion

We have constructed organic/inorganic hybrid materials consisting of thiol-functionalized isobutyl-POSS colloids and Au NPs. The key feature of the self-assembly of the hybrid is the crystallization of excess SH-POSS colloids, which form a fernlike thin film, with relatively large surface interstices that incorporate the SH-POSS-protected Au NPs. This simple, rapid,

droplet evaporation process allows thin films with ordered patterns to be prepared reproducibly with high quality. Moreover, Au NPs and SH-POSS colloids can be fused together through thermal treatment with essentially complete retention of the microwire structure—in this case, forming an interconnected porous bulk Au network. Given the simplicity and diversity of this method, we suspect that it may have several potential applications.

4. Experimental Section

Materials. 3-Mercaptopropyl isobutyl-POSS (SH-POSS) was purchased from Hybrid Plastics, Inc. 1-Dodecanethiol (SH-C12, >98%, Sigma-Aldrich), tetraoctylammonium bromide (TOAB, 98%, ACROS), hydrogen tetrachloroauate(III) trihydrate (HAuCl$_4$, ACS grade, ACROS), sodium borohydride (NaBH$_4$, >96%, Fluka), and HPLC-grade solvents were used as received.

Preparation of Au NPs. The molar feeding ratio (n/m) of HAuCl$_4$ to thiol compounds was the only controlling factor under the reaction conditions. SH-POSS and SH-C12 were selected to compare the effects of the protecting groups on the self-assembly of the Au NPs. A solution of HAuCl$_4$ (0.12 g) in water (100 mL, 6.03 mmol/L) was mixed with a solution of TOAB in toluene (6.03 mmol/L, 100 mL). The two-phase mixture was stirred vigorously until all the AuCl$_4^-$ ions were transferred into the organic layer. SH-POSS or SH-C12 was then added to the organic phase. Freshly prepared aqueous NaBH$_4$ (301.5 mmol/L, 100 mL) was slowly added with vigorous stirring. After further stirring for 3 h, the organic phase was separated, the toluene was evaporated using a rotary evaporator, and the residue was mixed with ethanol (400 mL) to remove excess TOAB. The mixture was maintained at −18 °C for 4 h, and then the dark brown precipitate was filtered off and washed twice with ethanol. The Au NPs of C12−Au (n/m = 1) and POSS−Au1 (n/m = 1) were obtained in yields of 53.75 and 36.31 wt %.

Analytical Procedures. For the TEM images, three drops of a toluene solution (40.9 μL; 10 mg/mL of POSS−Au1; 50 mg/mL of SH-POSS) were placed onto a water surface having a diameter of 5 cm. After air-drying at 25 °C for 30 min, the aggregates were transferred to a carbon-coated Cu TEM grid. For the AFM, SEM, and OM analyses, one drop of dilute toluene solutions (13.7 μL, 10 mg/mL of POSS−Au1, and 50 mg/mL of SH-POSS) was placed onto a wafer, and then they were air-dried at 25 °C.

Supporting Information Available: Experimental details; POSS crystallographic analysis; compositional analyses; TEM images of C12−Au and POSS−Au2; calculation of POSS-bilayer-protected 1.84 nm gold cores. This material is available free of charge via the Internet at http://pubs.acs.org.

References and Notes

(1) Huynh, W. U.; Dittmer, J. J.; Alivisatos, A. P. *Science* **2002**, *295*, 2425.

(2) Huang, X.; El-Sayed, I. H.; Qian, W.; El-Sayed, M. A. *J. Am. Chem. Soc.* **2006**, *128*, 2115.

(3) Salem, A. K.; Searson, P. C.; Leong, K. W. *Nat. Mater.* **2003**, *2*, 668.

(4) Patel, A. C.; Li, S.; Wang, C.; Zhang, W.; Wei, Y. *Chem. Mater.* **2007**, *19*, 1231.

(5) Glotzer, S. C.; Solomon, M. J. *Nat. Mater.* **2007**, *6*, 557.

(6) Love, J. C.; Urbach, A. R.; Prentiss, M. G.; Whitesides, G. M. *J. Am. Chem. Soc.* **2003**, *125*, 12696.

(7) Salant, A.; Amitay-Sadovsky, E.; Banin, U. *J. Am. Chem. Soc.* **2006**, *128*, 10006.

(8) Mokari, T.; Rothenberg, E.; Popov, I.; Costi, R.; Banin, U. *Science* **2004**, *304*, 1787.

(9) Caswell, K. K.; Wilson, J. N.; Bunz, U. H. F.; Murphy, C. J. *J. Am. Chem. Soc.* **2003**, *125*, 13914.

(10) Jackson, A. M.; Myerson, J. W.; Stellacci, F. *Nat. Mater.* **2004**, *3*, 330.

(11) Roucoux, A.; Schulz, J.; Patin, H. *Chem. Rev.* **2002**, *102*, 3757.

(12) Petit, C.; Taleb, A.; Pileni, M. P. *Adv. Mater.* **1998**, *10*, 259.

(13) Murray, C. B.; Kagan, C. R.; Bawendi, M. G. *Annu. Rev. Mater. Sci.* **2000**, *30*, 545.

(14) Andres, R. P.; Bielefeld, J. D.; Henderson, J. I.; Janes, D. B.; Kolagunta, V. R.; Kubiak, C. P.; Mahoney, W. J.; Osifchin, R. G. *Science* **1996**, *273*, 1690.

(15) Markovich, G. *Acc. Chem. Res.* **1999**, *32*, 415.

(16) Liu, J. *J. Am. Chem. Soc.* **1999**, *121*, 4340.

(17) Marinakos, S. M.; Brousseau, L. C., III; Jones, A.; Feldheim, D. L. *Chem. Mater.* **1998**, *10*, 1214.

(18) Whettern, R. L. *Acc. Chem. Res.* **1998**, *32*, 397.

(19) Boal, A. K.; Iihan, F.; DeRouchey, J. E.; Thurn-Albrecht, T.; Russell, T. P.; Rotello, V. M. *Nature* **2000**, *404*, 746.

(20) Li, B.; Ni, C.; Li, C. Y. *Macromolecules* **2008**, *41*, 149.

(21) Wang, G.; Murray, R. W. *Nano Lett.* **2004**, *4*, 95.

(22) Shenhar, S.; Rotello, V. M. *Acc. Chem. Res.* **2003**, *36*, 549.

(23) Sato, T.; Hasko, D. G.; Ahmed, H. *J. Vac. Sci. Technol.* **1997**, *B15*, 45.

(24) Lin, X. M.; Pathasarathy, R.; Jaeger, H. M. *Appl. Phys. Lett.* **2001**, *78*, 1915.

(25) Kannan, R. Y.; Salacinski, H. J.; Butler, P. E.; Seifalian, A. M. *Acc. Chem. Res.* **2005**, *38*, 879.

(26) Larsson, K. *Ark. Kemi* **1960**, *16*, 209.

(27) Waddon, A. J.; Coughlin, E. B. *Chem. Mater.* **2003**, *15*, 4555.

(28) Cui, L.; Collet, J. P.; Xu, G.; Zhu, L. *Chem. Mater.* **2006**, *18*, 3503.

(29) Miao, J.; Cui, L.; Lau, H. P.; Mather, P. T.; Zhu, L. *Macromolecules* **2007**, *40*, 5460.

(30) Sanyal, A.; Norsten, T. B.; Rotello, V. M. Nanoparticle−Polymer Ensembles. In *Nanoparticles: Building Blocks for Nanotechnology*; Rotello, V. M., Ed.; Kluwer: New York, 2004.

(31) Schmid, G.; Pugin, R.; Malm, J. O.; Bovin, J. O. *Eur. J. Inorg. Chem.* **1998**, 813.

(32) Wang, X.; Naka, K.; Itoh, H.; Chujo, Y. *Chem. Lett.* **2004**, *33*, 216.

(33) Naka, K.; Itoh, H.; Chujo, Y. *Bull. Chem. Soc. Jpn.* **2006**, *77*, 1767.

(34) Carroll, J. B.; Frankamp, B. L.; Srivastava, S.; Rotello, V. M. *J. Mater. Chem.* **2004**, *14*, 690.

(35) Carroll, J. B.; Frankamp, B. L.; Rotello, V. M. *Chem. Commun.* **2002**, *17*, 1892.

(36) van Herrikhuyzen, J.; George, S. J.; Vos, M. R. J.; Sommerdijk, N. A. J. M.; Ajayaghosh, A.; Meskers, S. C. J.; Schenning, A. P. H. J. *Angew. Chem., Int. Ed.* **2007**, *46*, 1825.

(37) Brust, M.; Walker, M.; Bethell, D.; Schiffrin, D. J.; Whyman, R. *J. Chem. Soc., Chem. Commun.* **1994**, 801.

(38) van Herrikhuyzen, J.; Janssen, R. A. J.; Meijer, E. W.; Meskers, S. C. J.; Schenning, A. P. H. J. *J. Am. Chem. Soc.* **2006**, *128*, 686.

(39) Mantz, R. A.; Jones, P. F.; Chaffee, K. P.; Lichtenhan, J. D.; Gilman, J. W.; Ismail, I. M. K.; Burmeister, M. J. *Chem. Mater.* **1996**, *8*, 1250.

(40) Liu, L.; Tian, M.; Zhang, W.; Zhang, L.; Mark, J. E. *Polymer* **2007**, *48*, 3201.

(41) Shigematsu, K. Crystal Growth of Alkali Salts from Concentrated Aqueous Solutions. In *Crystallization Processes*; Ohtaki, H., Ed.; John Wiley and Sons: New York, 1999; Vol. 3, pp 69−97.

(42) Jeong, K. U.; Knapp, B. S.; Ge, J. J.; Graham, M. J.; Tu, Y.; Leng, S.; Xiong, H.; Harris, F. W.; Cheng, S. Z. D. *Polymer* **2006**, *47*, 3351.

(43) Zhang, J. Z.; Wang, Z. L.; Liu, J.; Chen, S.; Liu, G. *Self-Assembled Nanostructures*; Kluwer Academic: New York, 2003.

(44) Krätschmer, W.; Lamb, L. D.; Fostiropoulos, K.; Huffman, D. R. *Nature* **1990**, *347*, 354.

(45) Kroto, H. W.; Heath, J. R.; O'Brien, S. C.; Curl, R. F.; Smalley, R. E. *Nature* **1985**, *318*, 162.

(46) Larsson, K. *Ark. Kemi* **1960**, *16*, 215.

(47) Chunyan, B.; Ming, J.; Ran, L.; Tierui, Z.; Yingying, Z. *Mater. Chem. Phys.* **2003**, *82*, 812.

(48) Fullam, S.; Cottell, D.; Rensmo, H.; Fitzmaurice, D. *Adv. Mater.* **2000**, *12*, 1430.

(49) Prevo, B. G.; Fuller, J. C., III; Velev, O. D. *Chem. Mater.* **2005**, *17*, 28.

(50) Xenogiannopoulou, E.; Iliopoulos, K.; Couris, S.; Karakouz, T.; Vaskevich, A.; Rubinstein, I. *Adv. Funct. Mater.* **2008**, *18*, 1281.